

Lab 3

1. Improved GPS Positioning

Whether it is noise or an atmospheric disturbances, GPS positioning inherently involves some error. To combat this error, different methods can be used to correct the raw measurements. In this section, different methods are used to correct the positioning of a static Novatel receiver. This receiver was located in the Auburn MRI, and data was taken on March 16, 2023 at a 1 Hz sample rate. To start, an initial GPS position solution for the static data set was determined using a Gauss-Newton least squares approach. The least squares equation is given as:

$$x = (G^T G)^{-1} G^T y \quad (1)$$

where x is the state vector including the position and clock bias differentials, G is the geometry matrix, and y is the difference between the pseudorange and range. To determine the static position solution, only the 8 satellites that had both L1 and L2 pseudoranges for the entire data set were used. This was done so that the amount of satellites used in each solution method would remain constant. Any improvements in positioning would be a consequence of removing error not removing or adding satellites. *Figure 1* gives the position solution for the static data set.

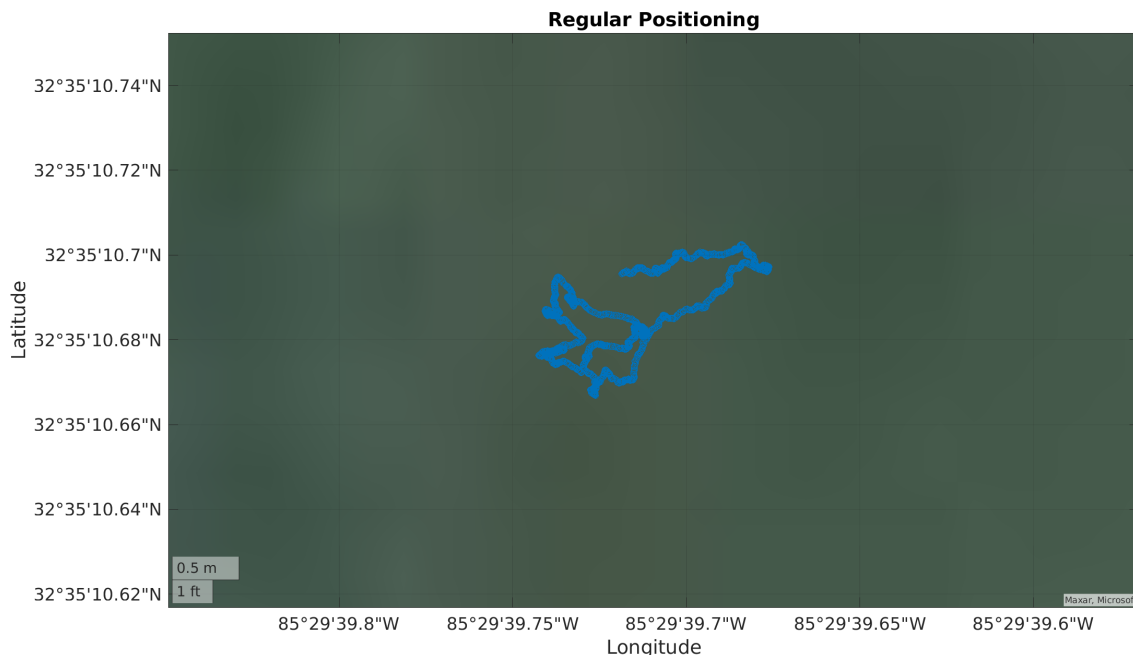


Figure 1: Static GPS Position Solution.

After determining the static GPS position solution carrier phase smoothing was performed to
Page 1 of 19

mitigate the measurement noise. Carrier phase smoothing utilizes the relative distance on a less noisy carrier phase measurement to average the pseudorange over a window. The equation for carrier phase smoothing is given as:

$$\bar{\rho}(t_i) = \frac{1}{M} \rho(t_i) + \frac{M-1}{M} [\bar{\rho}(t_i-1) + \phi(t_i) - \phi(t_i-1)] \quad (2)$$

where $\bar{\rho}$ is the averaged pseudorange, M is the averaging window, t_i is the current time step, and ϕ is the carrier phase. Increasing the averaging window allows for more smoothing but could introduce a bias. Therefore window sizes of 2, 8, and 15 minutes were used as averaging windows and compared against each other. To generate a position solution the same Gauss-Newton least squares method is used but with the averaged pseudorange. *Figure 2* shows the carrier phase smoothed GPS position solutions for each averaging window along with the regular GPS position solution.

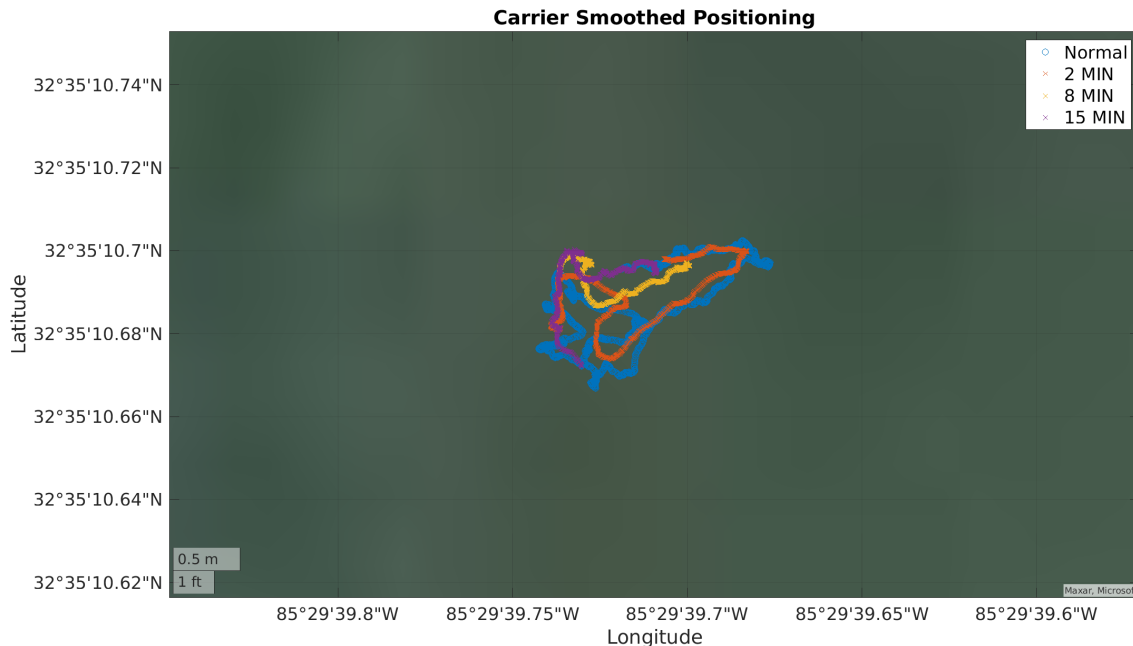


Figure 2: Carrier Smoothing GPS Position Solution.

From *Figure 2*, it can be seen that increasing the averaging window tightens the position solution. A smoother pseudorange measurement limits the amount of variance on the position solution. For the static scenario, an inclusion of a new bias is not seen for any of the averaging windows. Therefore, the higher 15 minute averaging window would be the preferred averaging window.

The next method used to reduce the static position error was implementing an ephemeris ionosphere error model. This method estimates the atmospheric error due to the ionosphere and removes it from the pseudorange measurements. The equation for calculating the ionosphere correction term, taken from the GPS Interface Control Document (https://eng.auburn.edu/~dmbevly/fund_gps/)

`IonosphereCorrectionAlgorithm.pdf`) is given as:

$$T_{iono} = \begin{cases} F * \left[5(10^{-9}) + AMP\left(1 - \frac{x^2}{2} + \frac{x^4}{24}\right) \right], & |x| < 1.57 \\ F * [5(10^{-9})] & |x| \geq 1.57 \end{cases} \quad (3)$$

where T_{iono} is the ionosphere correction term, F is the obliquity factor, and x is the phase. This ionosphere is subtracted from the pseudorange, and a new position solution is calculated. *Figure 3* shows the GPS position solution using the ephemeris ionosphere model correction as well as the original GPS position solution.

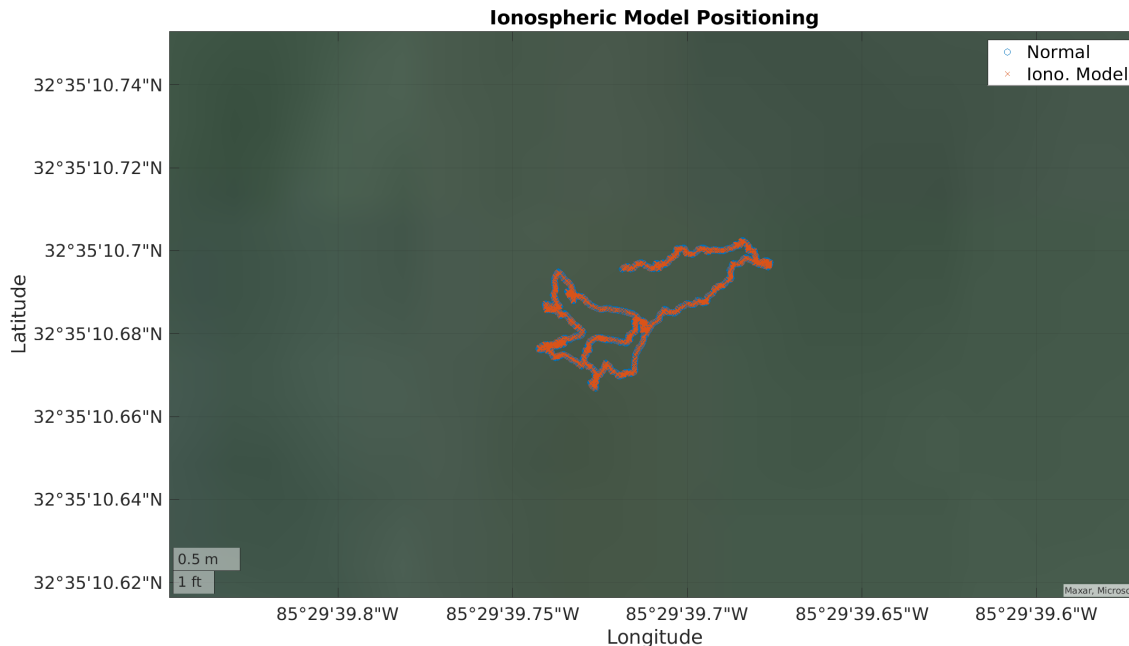


Figure 3: Ephemeris Model Correction GPS Position Solution.

The ephemeris ionosphere model correction did not have much of an effect on the position solution. This is due to low amounts of ionosphere error being present in the data set to begin with. Another method of mitigating the ionosphere error is to use dual frequency to produce ionosphere free measurements. The error due to the ionosphere differs based on the signal frequency. By comparing pseudorange measurements at different frequencies, the error due to the ionosphere can be ascertained. The equation for an ionosphere free pseudorange is given by:

$$\rho_{IF} = \frac{f_{L1}^2}{(f_{L1}^2 - f_{L2}^2)} \rho_{L1} - \frac{f_{L2}^2}{(f_{L1}^2 - f_{L2}^2)} \rho_{L2} \quad (4)$$

where ρ_{IF} is the ionosphere free pseudorange, f_{L1} is the L1 frequency, and f_{L2} is the L2 frequency. This ionosphere free pseudorange is used to create a new position solution. *Figure 4* shows the GPS position solution using the dual frequency ionosphere free measurements and the original

position solution.

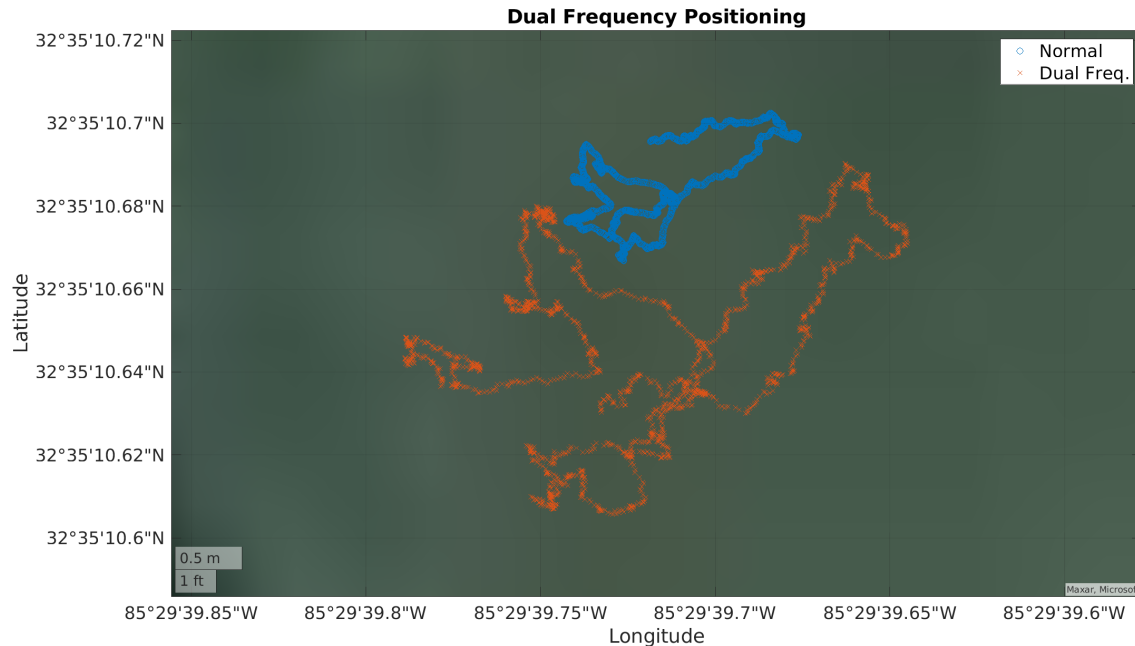


Figure 4: Dual Frequency Ionosphere Free GPS Position Solution.

From *Figure 4* it can be seen that the position solution with the ionosphere free measurements moves to a new general location. This is due to the removal of the ionosphere error. However, it is also shown that the new position solution is scattered much more when compared to the original position solution. Since the error is added from both the L1 and L2 signals, the position solution will show more variance.

Each of the static positions solutions are plotted against each other in *Figure 5*. Additionally, *Table 1* gives the mean position in latitude and longitude as well as the standard deviation of the ECEF positions.

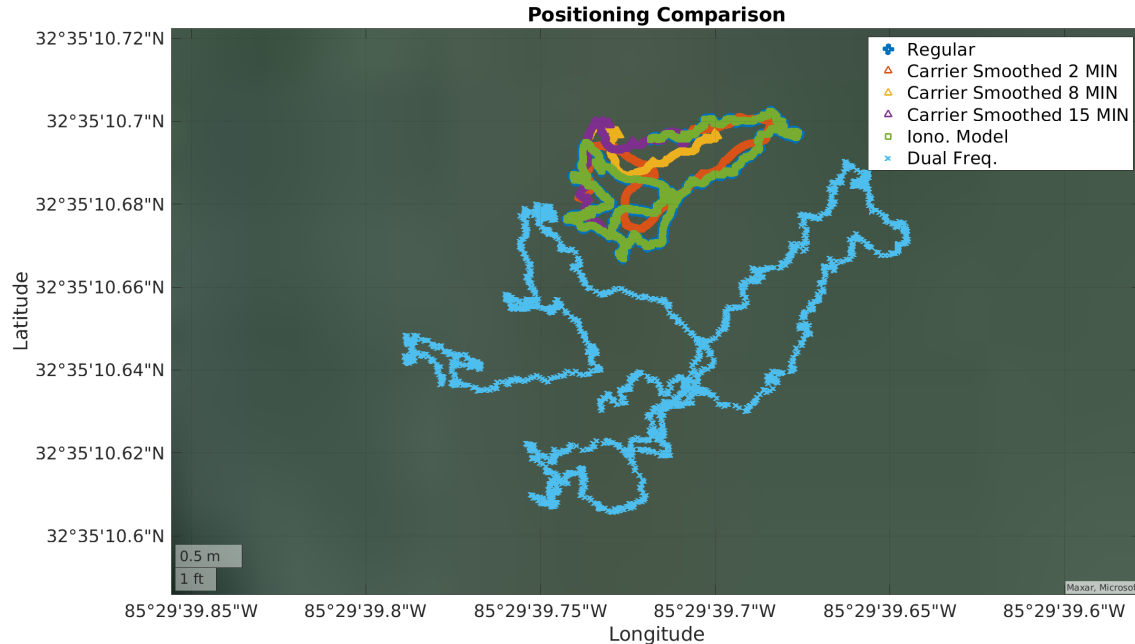


Figure 5: Dual Frequency Ionosphere Free GPS Position Solution.

Table 1: Statistics for Static Position Solutions.

	μ_ϕ (°)	μ_λ (°)	σ_x (m)	σ_y (m)	σ_z (m)
Regular					
L1 Position	32.586302	-85.494366	0.533	0.651	0.734
Carrier Smoothing					
2 min	32.586302	-85.494366	0.509	0.553	0.624
8 min	32.586303	-85.494368	0.362	0.191	0.318
15 min	32.586304	-85.494369	0.245	0.253	0.245
Ionosphere Correction					
Ephemeris Model	32.586302	-85.494366	0.533	0.652	0.734
Dual Frequency	32.586291	-85.494367	0.946	1.391	1.252

From *Figure 5* and *Table 1* it can be seen that each of the position solutions are located in a similar location. The only position solution that is located farther than 1 meter away from the others is the dual frequency position solution. The dual frequency positioning is on average about 8 meters away from the original positioning solution. This is due to the removal of the ionosphere error, which removes a bias in the measurements. However, this position solution also has the highest standard deviation. This is due to the noise on the measurements being increased since two different pseudoranges are used. The positioning solution with the lowest standard deviation is the carrier smoothed positioning solution with a 15 minute averaging window. The noise on the measurements was mitigated using the more precise carrier phase measurements, leading to less

position variance. The ionosphere model position solution has the least amount of impact on the original solution. The mean and standard deviation for each position solution are about the same. This is because the calculated ionosphere correction term was small for the entire data set. To remove both the noise and bias on the original position solution, using a mix of the dual frequency and carrier smoothing methods would be the most ideal.

2. Static Relative DGPS Positioning

Differential GPS (DGPS) techniques can utilize the same techniques used in single receiver positioning. To begin, a single receiver positioning solution was done using *Equation 1* as a baseline for all DGPS techniques. This is presented in *Figure 6*. Note that for this entire section, two receivers were connected to the same antenna, therefore the distance between the receivers should be 0 meters.

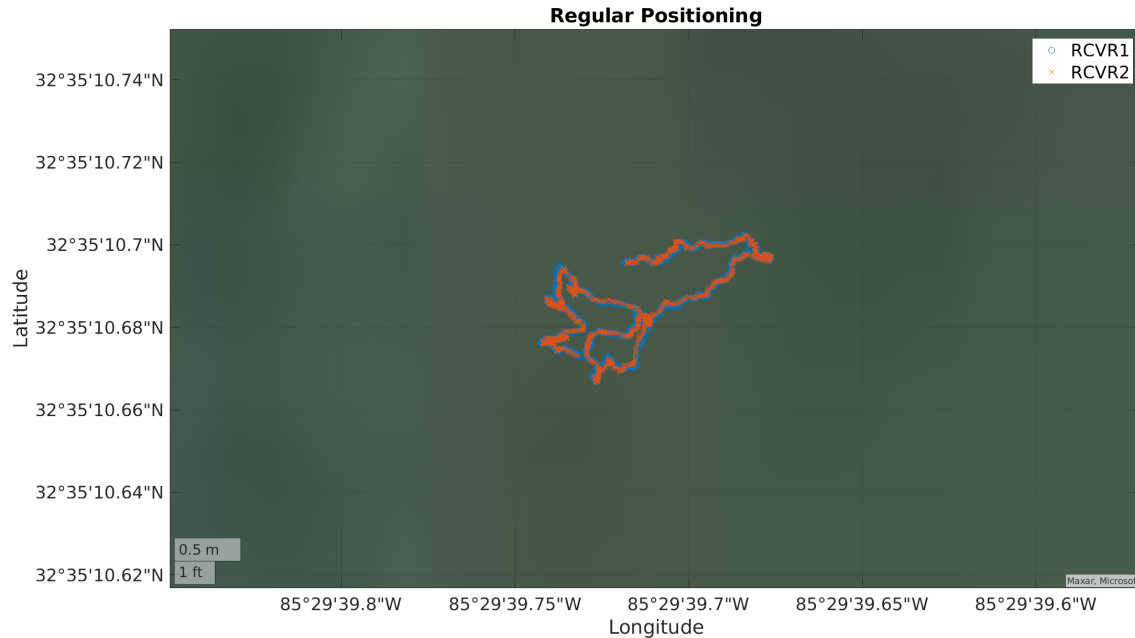


Figure 6: Static Position of Two Receivers.

Next, the DGPS solution was created using RCVR_S2 as the base station. This was determined via the linear least squares solution below.

$$\delta\rho = \begin{bmatrix} u_x & u_y & u_z & 1 \end{bmatrix} \begin{bmatrix} r_x \\ r_y \\ r_z \\ c\delta t \end{bmatrix} \quad (5)$$

Where $\delta\rho$ is the pseudorange difference between the receivers, u are the unit vectors of one

receiver to the satellites, r are the relative position vectors from the first receiver to the second, and $c\delta t$ is the clock bias difference between the receivers. *Figure 7* shows the DGPS solution when using RCVR_S2 as the base station.

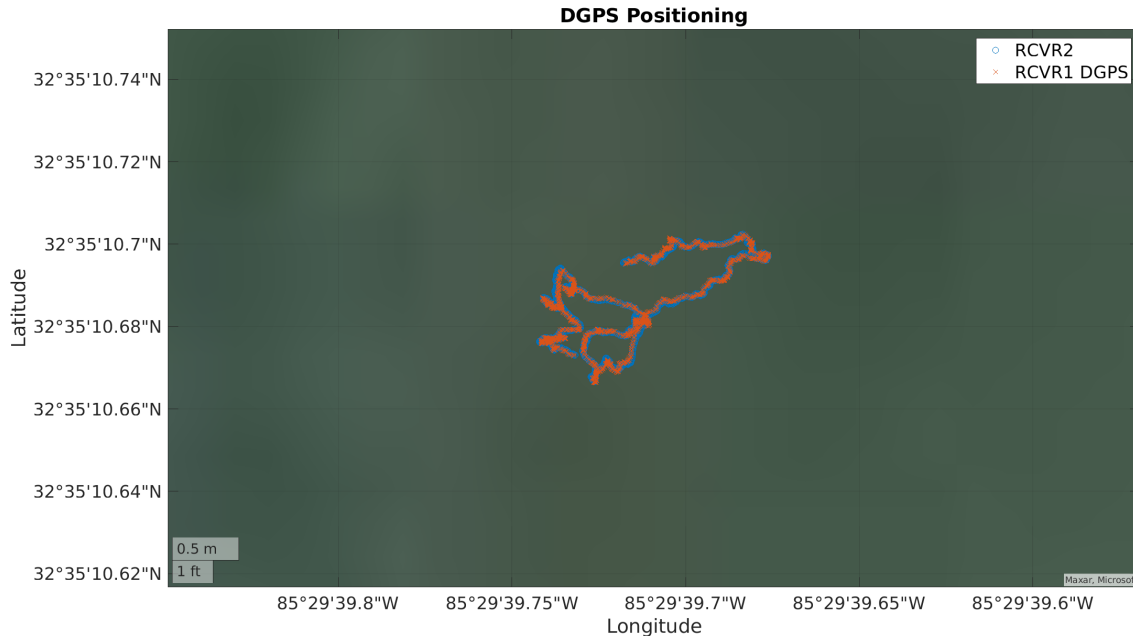


Figure 7: Static DGPS Solution.

As shown, the DGPS solution is almost identical to the reference solution as the baseline between them is 0 meters and both receivers are connected to the same antenna.

Carrier phase smoothing was again utilized to mitigate the measurement noise on the pseudorange measurements. This time, however, the psuedorange and carrier differences between the measurements were used as shown in *equation 6*.

$$\delta\bar{p}(t_i) = \frac{1}{M} \delta\rho(t_i) + \frac{M-1}{M} [\delta\bar{p}(t_{i-1}) + \delta\phi(t_i) - \delta\phi(t_{i-1})] \quad (6)$$

Sizing widows of 2, 8, and 15 minutes were used and presented in *Figure 8*. The smoothing attempt on the DGPS solution has no visual impact on the positioning solution, likely due to the small differences in the measured psuedoranges and carrier from the receivers which leads to the smoothing having minimal effect on the solution.

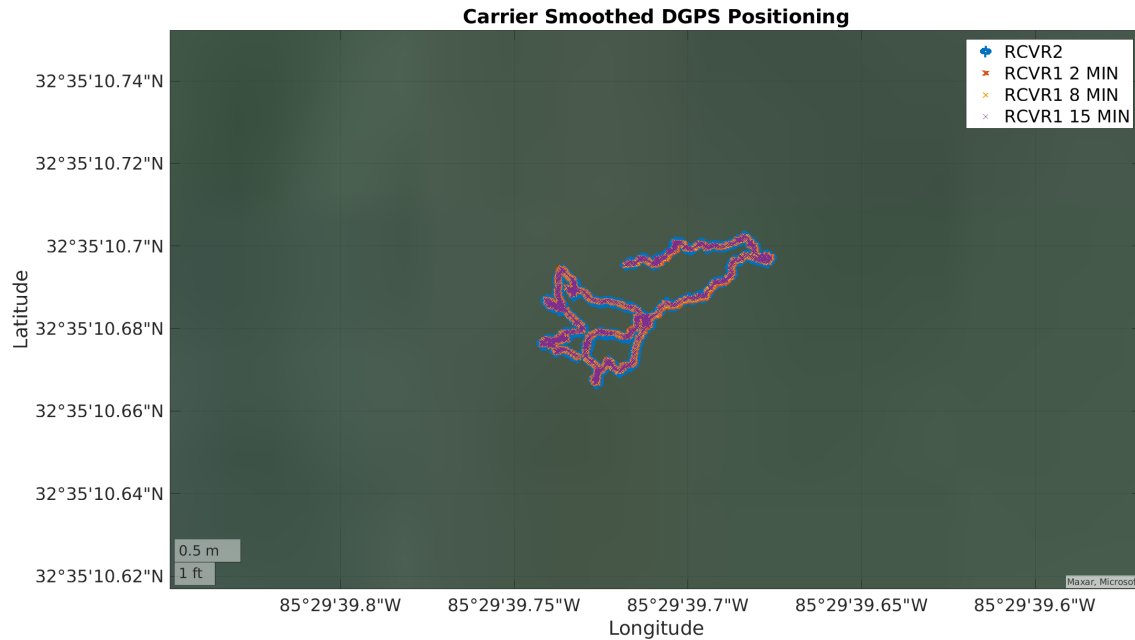


Figure 8: Static Carrier Smoothed DGPS Solution.

Lastly, a RTK DGPS solution was used to position the two receivers. This utilized carrier measurements by attempting to first estimate the integer ambiguity seen in the measurement as shown.

$$\delta\phi = \begin{bmatrix} u_x & u_y & u_z & 1 \end{bmatrix} \begin{bmatrix} r_x \\ r_y \\ r_z \\ c\delta t \end{bmatrix} + \lambda\delta N = G\delta r + \lambda\delta N \quad (7)$$

Where λ is the carrier wavelength and δN is the estimated integer ambiguity between the receivers. Using the L1 pseudorange measurement along with the L1 and L2 carrier measurements, the integer ambiguity can be solved for as follows:

$$\begin{bmatrix} \delta\rho_{L1} \\ \delta\phi_{L1} \\ \delta\phi_{L2} \end{bmatrix} = G\delta r + \begin{bmatrix} 0 & 0 \\ \lambda_{L1} & 0 \\ 0 & \lambda_{L2} \end{bmatrix} \begin{bmatrix} \delta N_{L1} \\ \delta N_{L2} \end{bmatrix} \quad (8)$$

Separating the second half of the equation and solving for the integer ambiguity:

$$\begin{aligned} L &= \text{leftnull}(G) \\ \delta N &= [(L\lambda)^T(L\lambda)]^{-1}(L\lambda)^T L y \\ P_{\delta N} &= [(L\lambda)^T(L\lambda)]^{-1} \end{aligned} \quad (9)$$

This hand solution is a medium fidelity, potential solution, however, the Lambda method was

employed on this solution to provide an even more accurate solution. This solution was implemented with the code provided by Delft University. *Figure 9* is a plot of the RTK DGPS solution from the Lambda method, which again shows little visual improvement over the reference solution.

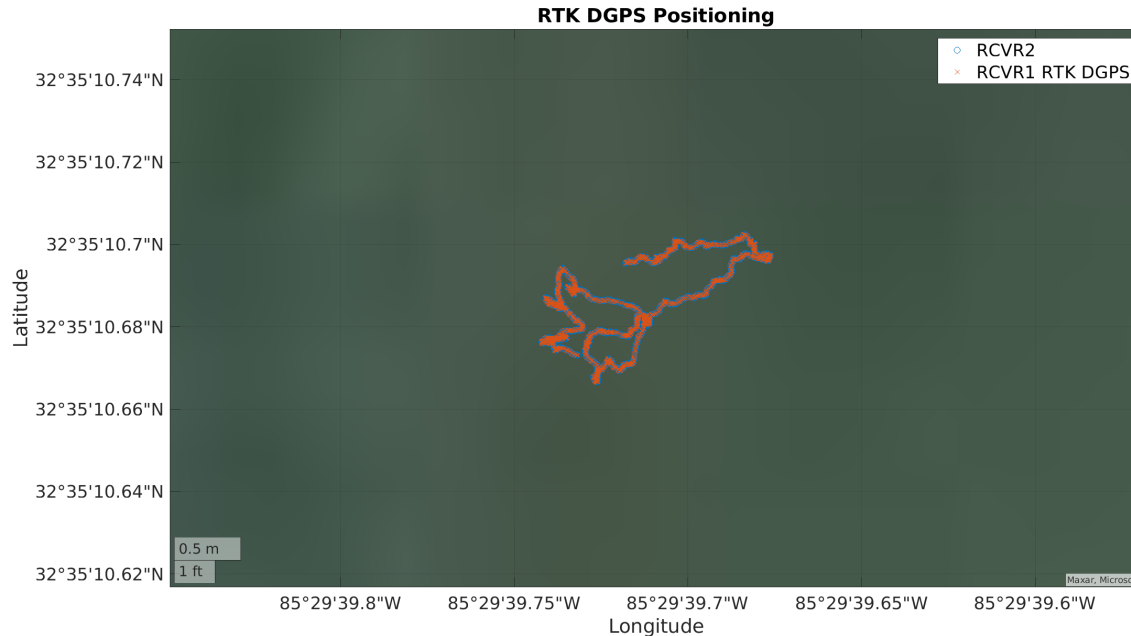


Figure 9: Static RTK DGPS Solution.

The statistics on the position difference between the receivers for each static DGPS method are tabulated in *Table 2* and shown in *Figure 10*. These were taken on the distance magnitude between the receivers.

Table 2: Statistics for Static DGPS Position Difference.

	$\mu(m)$	$\sigma(m)$
Reference		
L1 Position	0.023808	0.012676
DGPS		
Pseudorange	0.023808	0.012676
Carrier RTK	0.000486	0.000309
Carrier Smoothing DGPS		
2 min	0.010486	0.006701
8 min	0.006056	0.003862
15 min	0.006582	0.003554

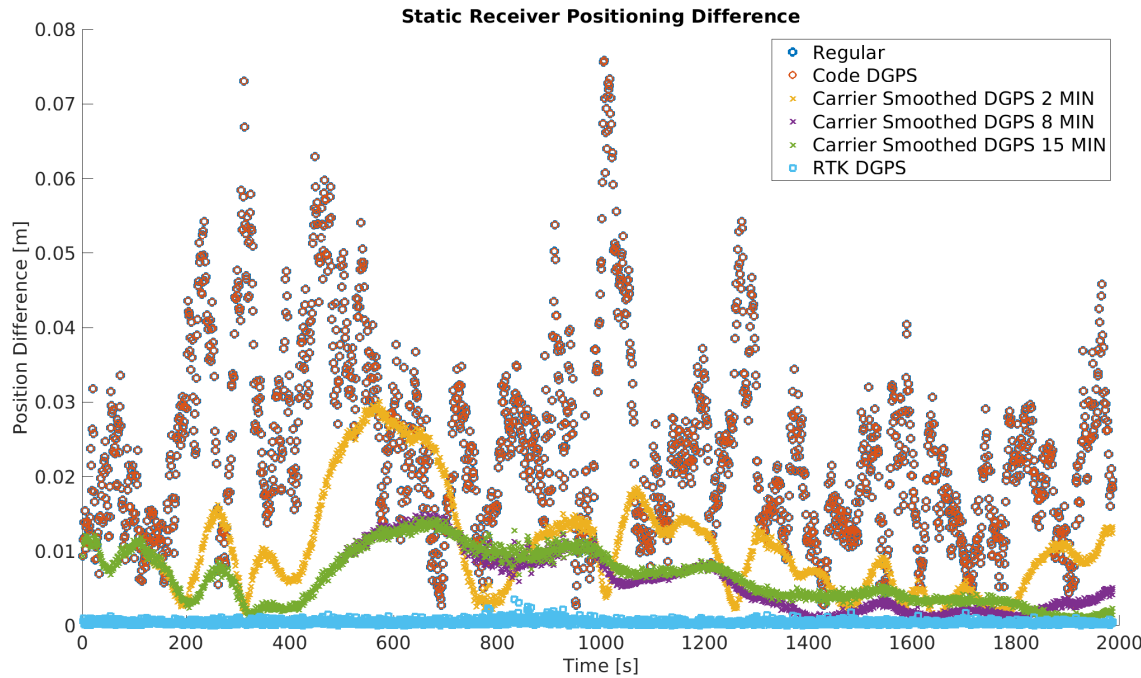


Figure 10: DGPS Relative Position Vector Over Time.

As shown by the statistics, the RTK Positioning solution is by far the superior static DGPS positioning method. This is due to the cleanliness of the carrier measurement such that when using it to position provides an extremely clean solution with little noise. The mean of this solution is less than $5(10^{-4})$ which is essentially 0. This carrier effect is also shown in the carrier smoothing technique as the carrier greatly smooths out the psuedorange measurements leading their error to be reduced by over 50%. It is also apparent that the Code (psuedorange) DGPS solution is the exact same as the independent receiver positioning. This is likely due to the receiver setup as both are receiving measurements via the same antenna.

3. Dynamic Relative DGPS Positioning

The same DGPS solutions that were evaluated for two static receivers were then performed with two dynamic receivers. This time however, each receiver had their own antenna and had a static distance of 50 inches (1.27 meters) between them. Also note, for the dynamic DGPS solutions, there were a few occurrences where both receivers did not have a common 4 satellites in view, which were removed from the simulation. The original GPS position solutions for both receivers were plotted against each other in *Figure 11*. The original GPS positions solutions were found using the least squares method discussed in *equation 1*.

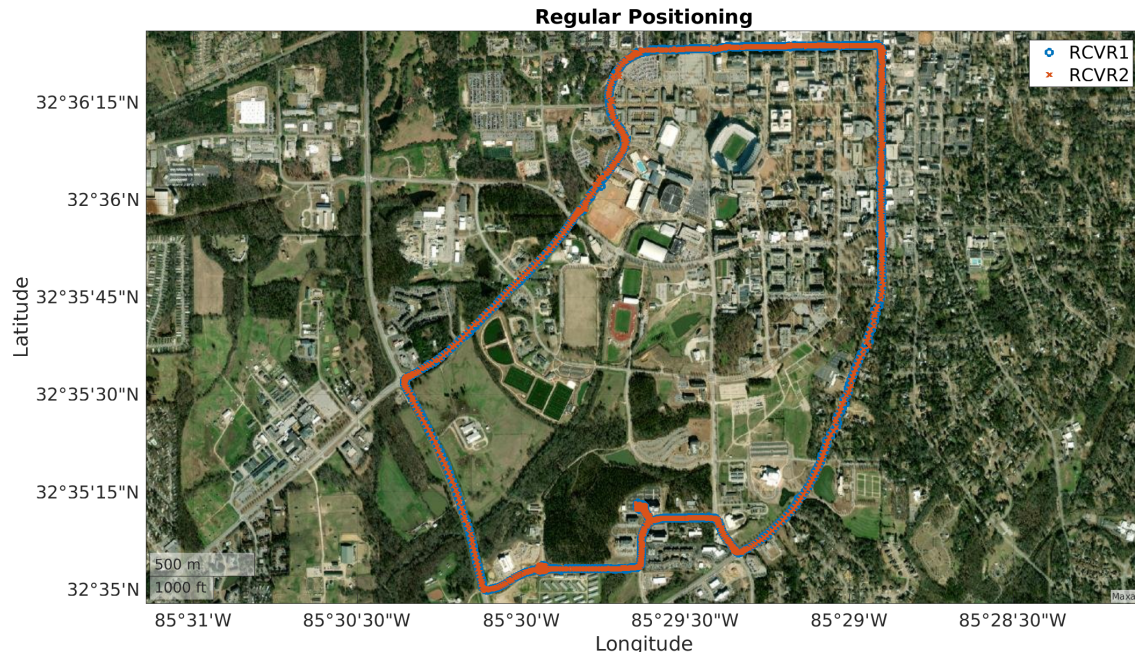


Figure 11: Original Dynamic GPS Position Solutions.

Without using any form of DGPS the difference in position solutions between the two receivers is somewhat large. The position difference between the two receivers should only be 1.27 meters apart, but the mean position difference is over 7 meters. To eliminate this error and variance different methods of DGPS positioning are performed with the second receiver acting as the base.

To start, code DGPS is performed using *equation 5*. In addition to this, since the distance between the receivers is static, the least squares solution for the distance between the receivers was performed recursively to reduce spikes in error. In recursive estimation, the covariance matrix is maintained across time epochs leading to any new information being smoothed out by the uncertainty of prior measurements along with the uncertainty of the new measurement. The position solution for both code DGPS positions are shown on *Figure 12* alongside the original dynamic position solution.

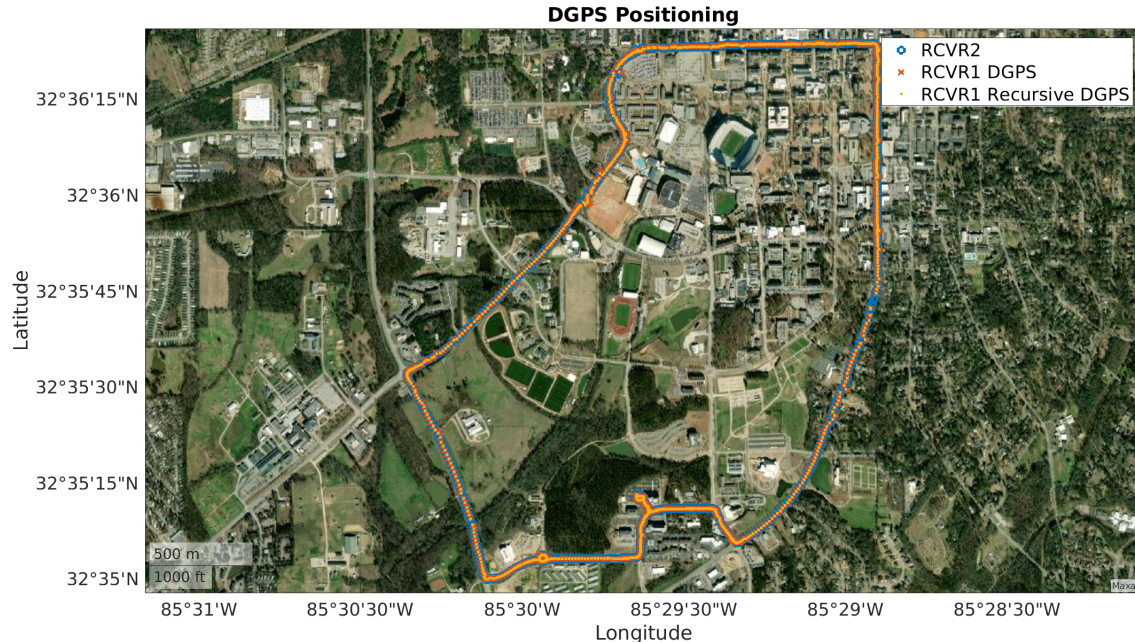


Figure 12: Dynamic Code DGPS Position Solution.

Implementing code DGPS significantly decreases the difference between the receivers. Any error due to the atmosphere are removed from the pseudorange measurements. Additionally, recursive DGPS decreased the position error even more with a 1.6 meters of position difference and a 0.4 meter standard deviation. Recursive estimation combats areas of bad measurements by using the prior time epochs covariance matrix.

Carrier phase smoothing DGPS was then performed on the dynamic data using *equation 6*. Averaging windows of 2, 8, and 15 minutes were evaluated as potential time windows. Averaging was done with any satellite available for each time step. Each satellite was individually smoothed while in view and smoothing was restarted any time the satellite left view. *Figure 13* gives the carrier phase smoothing DGPS dynamic position solution plotted against the original position solution.

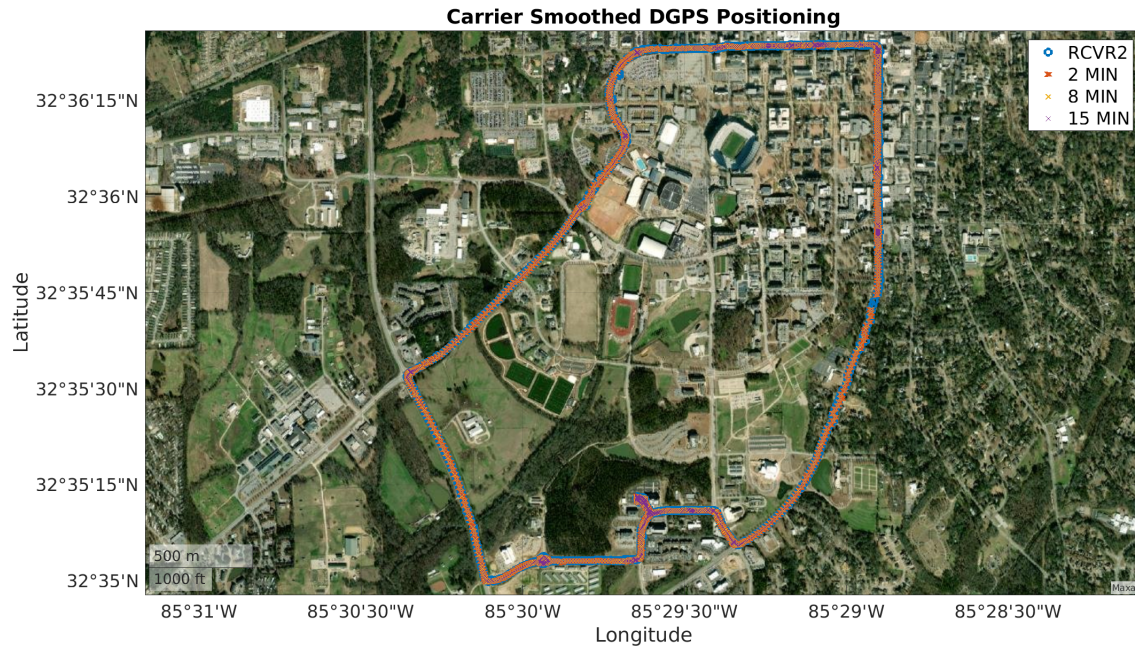


Figure 13: Dynamic Carrier Phase Smoothed DGPS.

Each of the carrier phase smoothed DGPS position solutions decreased the amount of range error in the measurements. Additionally, increasing the averaging window decreased the amount of variance on the measurements. The 15 minute averaging window never introduced a bias on the measurements, so it was the preferred averaging window. Using the more precise carrier measurements mitigated the noise on the pseudorange measurements.

A RTK DGPS position was then computed using *equations 7-9*. The integer ambiguities were approximated using the Lambda method to increase fidelity. *Figure 14* gives the dynamic RTK DGPS position solution. Measurements were used at time epochs where there were measurements available for both the L1 and L2 frequencies.

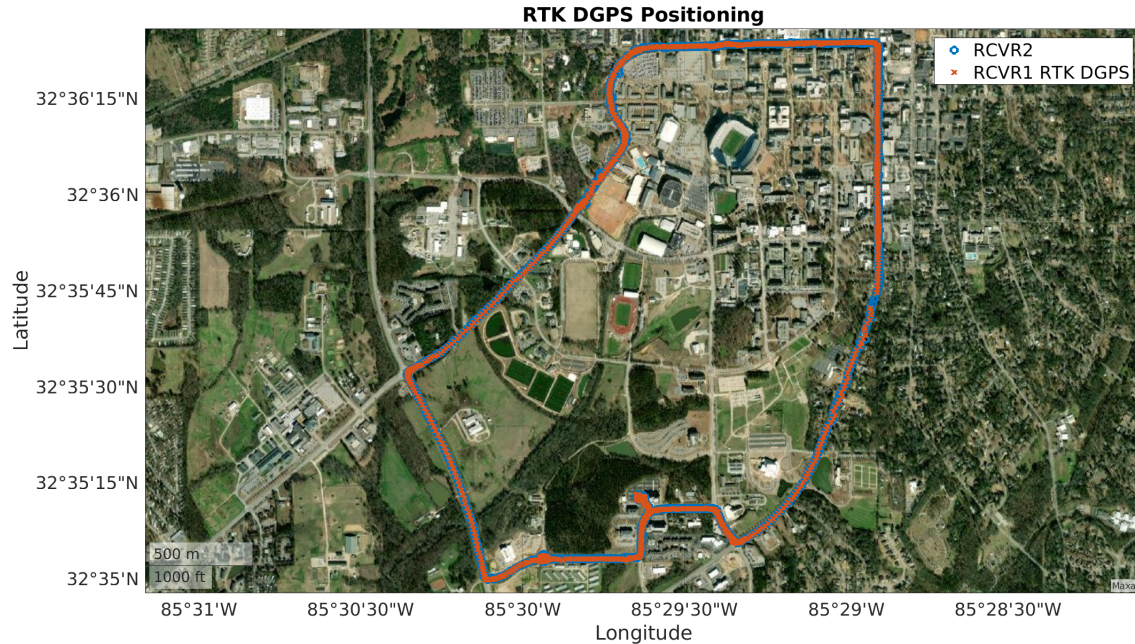


Figure 14: Dynamic RTK DGPS.

The RTK DGPS solution improved the range error. Using the more precise carrier phase measurement mitigates the noise on the measurements. Additionally, the DGPS removes the atmospheric error. However, the RTK DGPS sometimes spikes in error. This is due to the integer ambiguities being imprecise to measure when measurements are corrupted. Additionally, some carrier phase measurements have to be thrown out when the difference between measurements drastically increased.

Figure 15 shows the range error for each DGPS method over time. Table 3 shows the mean and standard deviation of the ranging errors for each DGPS position solution.

Table 3: Statistics for Static DGPS Position Difference.

	$\mu(m)$	$\sigma(m)$
Reference		
L1 Position	6.476002	7.177811
DGPS		
Psuedorange	4.452806	4.452806
Recursive	1.627683	0.413855
Carrier RTK	4.452835	4.755819
Carrier Smoothing DGPS		
2 min	4.452806	4.750667
8 min	3.941766	3.114561
15 min	3.361717	2.972168

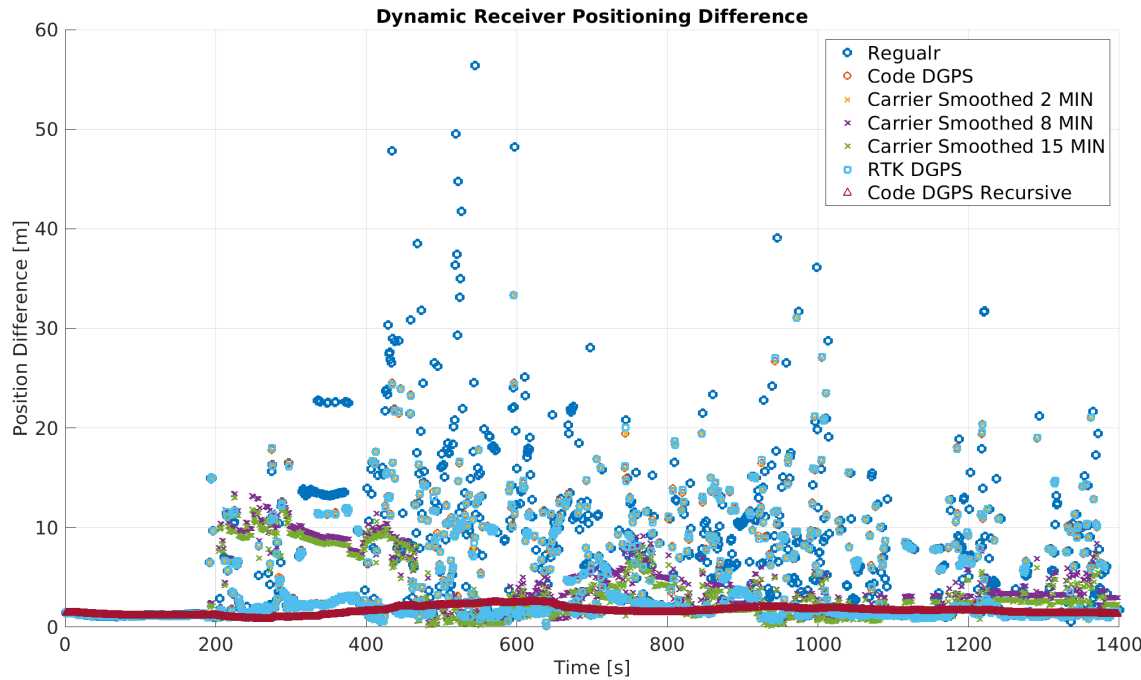


Figure 15: Range Error Comparison of Dynamic DGPS.

From the figure and table it is shown that the recursive code DGPS is the optimal method or error mitigation for the dynamic data set. It had the lowest mean range error, and also displayed the least amount of variance. DGPS eliminates the atmospheric error while the recursive elements smooth the results since the distance between the receivers should remain constant. The 8 and 15 minute carrier smoothing position solution also gave solutions with low range error and variance. The cleaner carrier phase measurements helped to control the noise on the pseudorange measurements while also getting the added effects if DGPS. While every method reduced the range error, the normal code DGPS, RTK DGPS, and 2 minute carrier smoothed solution experienced considerable variance. In each of these methods, there was no control on the noise of the measurements. Since the data was taken while moving, the quality of the measurements was inherently worse. It should also be noted that the integer ambiguity estimated for the RTK DGPS solution was sporadic due to poor quality measurements.

DGPS was also used to deduce the vehicle attitude during the run. The equation to solve for the azimuth using DGPS is given as:

$$\psi = \tan^{-1} \left(\frac{\delta E}{\delta N} \right) \quad (10)$$

where ψ is the azimuth, δE is the east distance between the two receivers, and δN is the north distance between the two receivers. The distance between the two receivers is the calculated relative position vector using the recursive code DGPS. This DGPS solution method was used

because it displayed the most accurate results for the dynamic scenario. The calculated azimuth was plotted against the GPS course derived from GPS velocity given in *equation 11* in *figure 16*. To match the frames as closely as possible, the azimuth was rotated by 15 degrees.

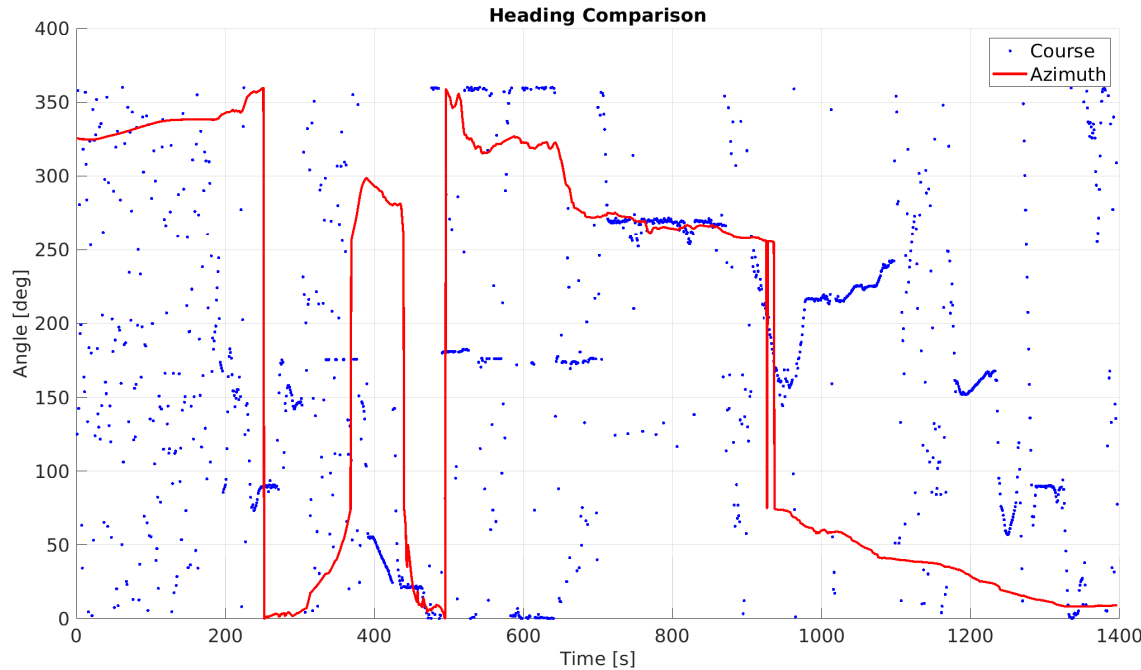


Figure 16: Azimuth vs GPS Course.

$$\psi = \tan^{-1} \left(\frac{\dot{E}}{\dot{N}} \right) \quad (11)$$

The calculated azimuth roughly matches the GPS course. While the trends are the same, the exact values do not always line up. The bias and variance on the DGPS solution certainly account for some of this error. The course measurements are also heavily predicated on the raw measurements of the base receiver. Corrupted measurements could greatly effect the course solution. Stopped motion also hurts the comparison, as the calculated azimuth will yield results while the GPS course will not. This is due to the GPS course being calculated based on velocity.

4. LAAS DGPS Positioning

In this section, the same DGPS solution techniques explored in previous parts were used, but in a more practical scenario. The position solution for a dynamic receiver is calculated using a static receiver as a base. To start, GPS position solutions were determined for both the static and dynamic receiver. This was done using the least squares method discussed in *equation 1*. *Figure 17* shows the standalone position solutions for both receivers. It is important to note that the receiver measurements were time synced using GPS time.

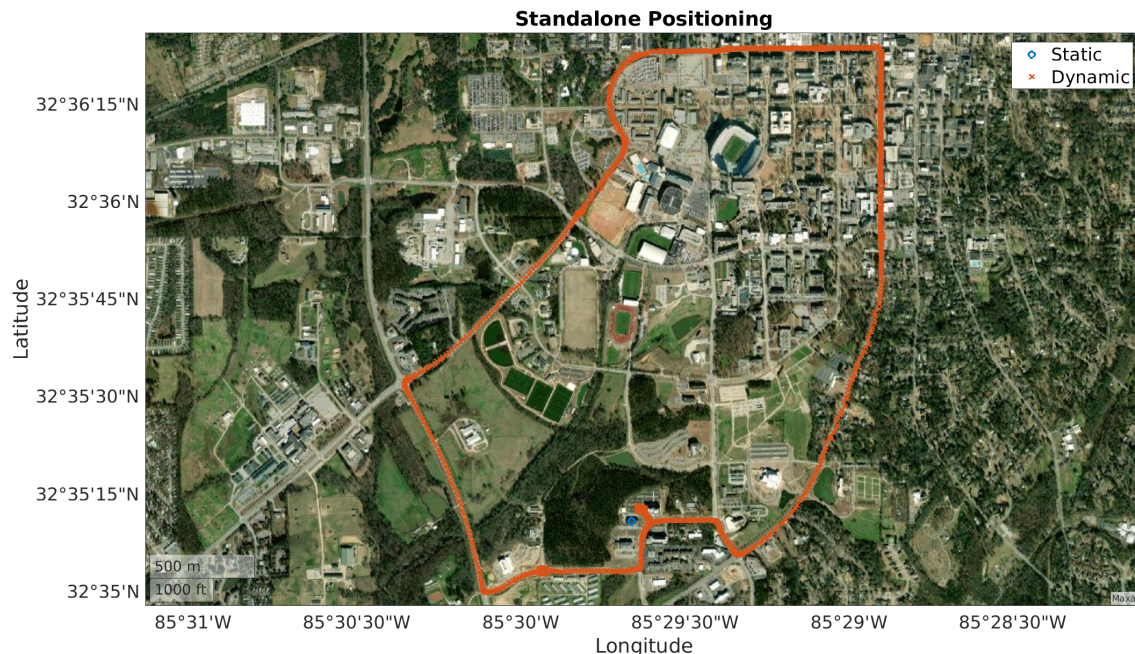


Figure 17: Standalone GPS Positioning Solutions.

From *Figure 18* it can be seen that the static data was taken at the Auburn MRI building while the dynamic data was taken on a path around Auburn's campus. Code DGPS was then performed between the dynamic and static receivers using *equation 5*. The position solution for this code DGPS is shown on *Figure 18*. Additionally, *Figure 19* gives the ECEF difference over time between the original and code DGPS dynamic position solutions.

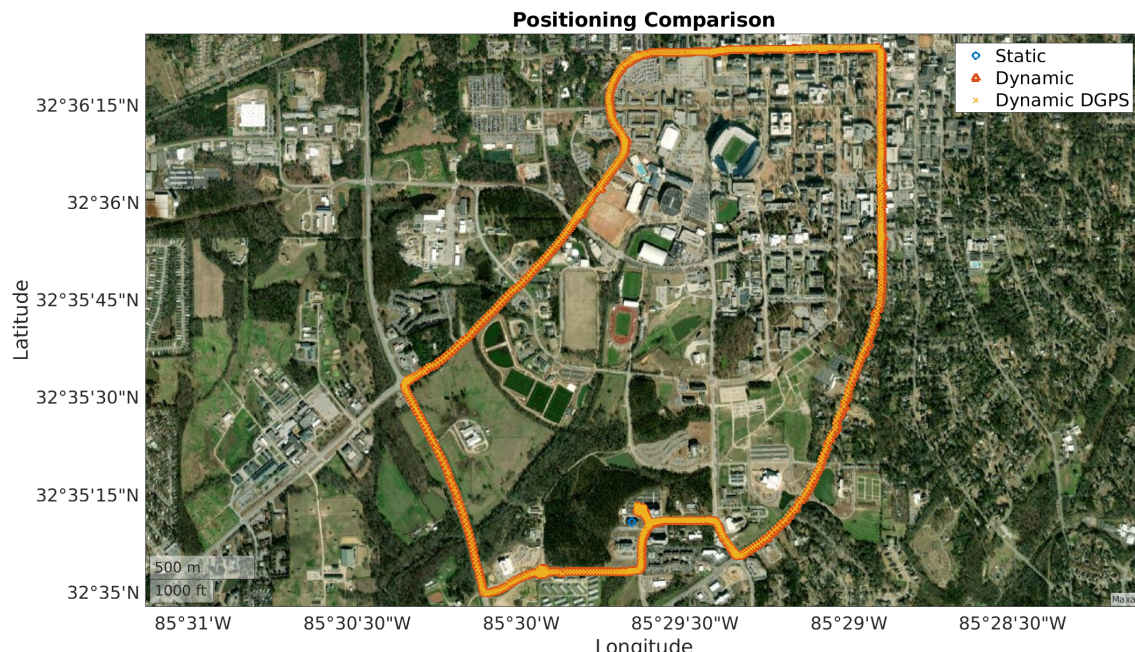


Figure 18: Code DGPS Positioning Solution.

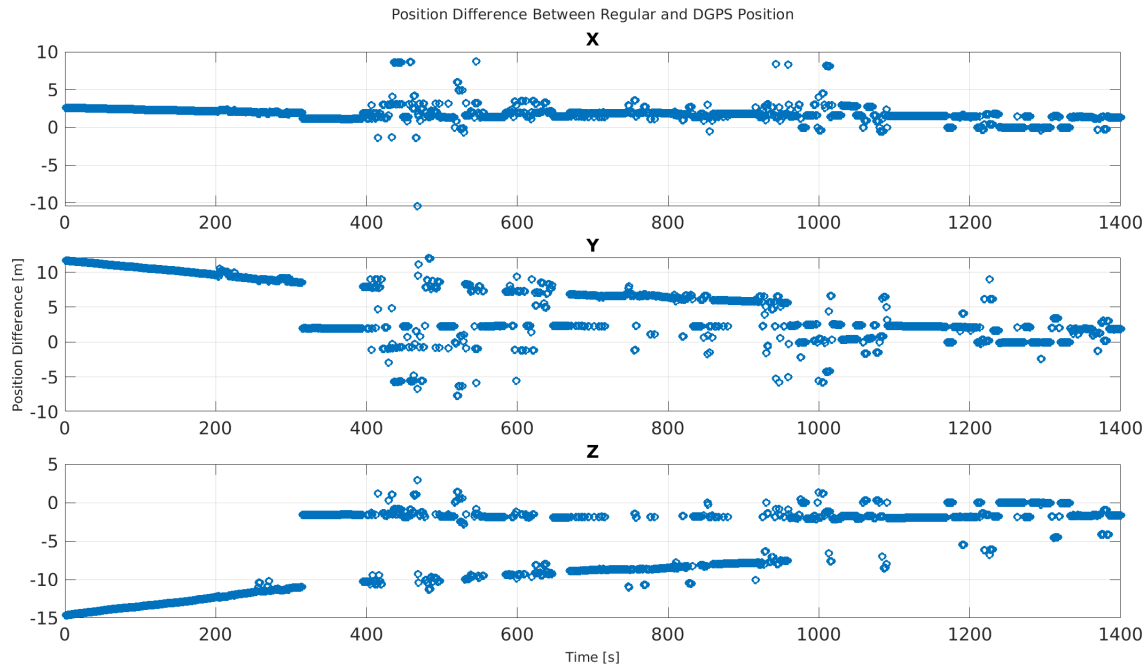


Figure 19: ECEF Position Difference Over Time.

From *Figures 19 and 20* it can be seen that the code DGPS solution closely follows that of the original position solution. The difference in position never goes above 15 meters of difference. This period of largest difference also occurs at beginning of the run during a long period of no movement. In these static scenarios, the code DGPS solution drifts since it has a greater noise component. Most of the differences in positions while moving between the two methods occurs during turns or periods of terrain blockage. During these instants, the code DGPS solution sticks onto the road as the original position solution drifts away. This can be seen better in *Figure 21* where the DGPS position solution stays on the road during tree blockage. It should also be noted that there are greater differences in the y-direction than the x direction. This is likely due to the satellites being more visible in that direction during the run, leading to less drift in that direction.

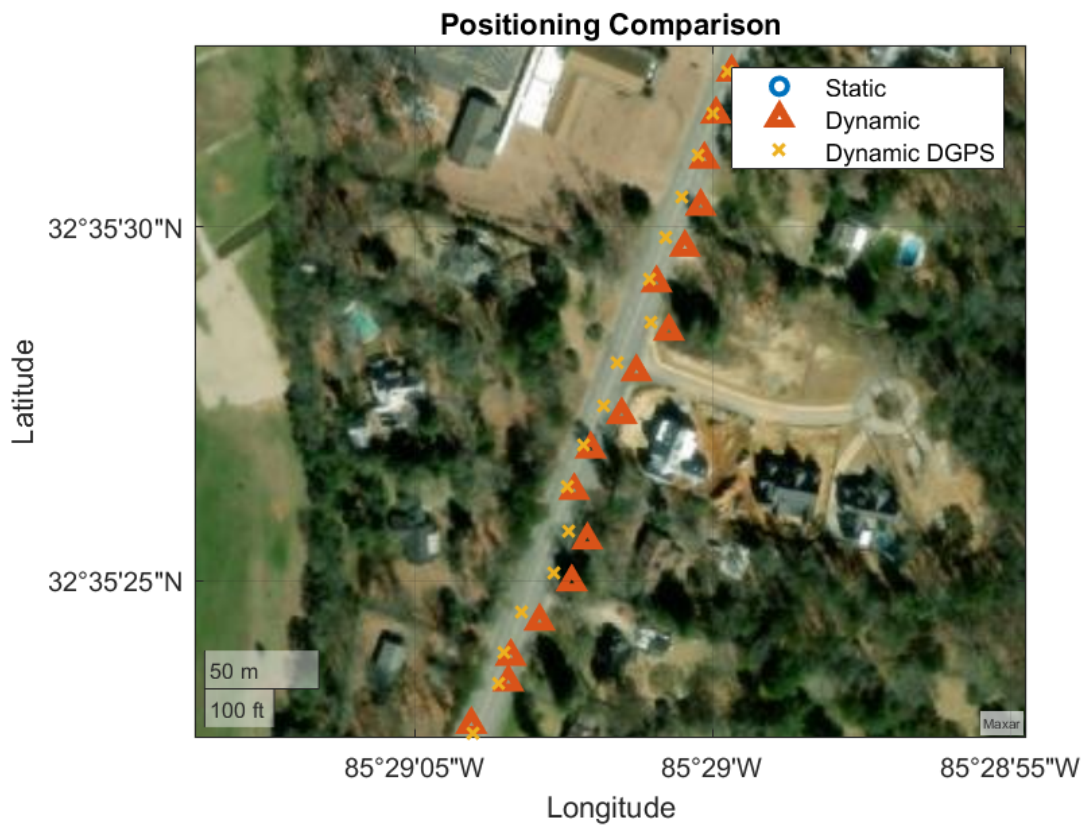


Figure 20: Zoomed in Comparison of Code DGPS and Original Position Solutions.